Available online at www.sciencedirect.com

ScienceDirect

Energy Procedia 43 (2013) 54 – 65

Energy Procedia

4th Workshop on Metallization for Crystalline Silicon Solar Cells

New selective processing technique for solar cells

M. Balucani[1,2,*] K. Kholostov[1], P. Nenzi[1], R. Crescenzi[1], D. Ciarniello[2], D. Bernardi[3], L. Serenelli[4], M. Izzi[4], M. Tucci[4]

[1] *DIET-Sapienza University of Rome, Via Eudossiana, 18 - 00184 Roma (ITALY)*
[2]*Rise Technolgy S.r.l. Lung. P. Toscanelli, 170- 00121 Roma (ITALY)*
[3]*2BG S.r.l. Via Monte Bianco, 18 - 35018 San Martino di Lupari (PD) (ITALY)*
[4]*ENEA Casaccia Research Centre Rome, Via Anguillarese 301, 00123, ITALY*

Abstract

A new selective processing technique based on a confined dynamic liquid drop\meniscus is presented. This approach is based on localized wet treatment of silicon wafers using confined and dynamic liquid drop that while in contact with the wafer forms a dynamic liquid meniscus. Such new technique allows to touch in specific defined positions the silicon wafer (front and/or back) in order to perform any kind of wet processing without the need of protective photo-resist. The new selective processing technique allows the metallizations (front and back) of mono and multi crystalline silicon solar cells. The front grid contacts are obtained by locally etching the silicon nitride, forming in a thin layer of meso-porous silicon and totally filling the meso-porous layer by pulse reverse plating a Nickel film. Copper and Tin are then electroplated using the same selective processing. This technology provides an effective solution to avoid silver pastes for front contact grid, as it guarantees low specific contact resistivity (550 $\mu\Omega cm^2$ on a 75 Ω/□ n-type doped emitter) and good adhesion to the silicon substrate (i.e. greater than 550 g/mm). The Al back side of the solar cell are also treated by the new selective process. Tin is directly deposited on Aluminum back contact showing adhesion higher than silver on silicon (i.e. > 1N/mm).

© 2013 The Authors. Published by Elsevier Ltd. Open access under CC BY-NC-ND license.
Selection and peer-review under responsibility of Guy Beaucarne, Gunnar Schubert and Jaap Hoornstra

Keywords: plating, liquid meniscus, solar cell, localized wet processing

* Corresponding author. Tel.: +39-06-96848773; fax: +39-06-96848774.
E-mail address: marco.balucani@risetechnology.com

1876-6102 © 2013 The Authors. Published by Elsevier Ltd. Open access under CC BY-NC-ND license.
Selection and peer-review under responsibility of Guy Beaucarne, Gunnar Schubert and Jaap Hoornstra
doi:10.1016/j.egypro.2013.11.088

1. Introduction

In silicon solar cell based module the cost per watt composition is given for approximately 29% from the semiconductor part (i) (i.e. Si feedstock, saw wires, saw slurry, equipment, labor, cost of capital, manufacturing margin, etc.), about 22% from the cell fabrication cost (ii) (i.e. metallization, SiN_x, dopant, chemicals, equipment, labor, cost of capital, manufacturing margin, etc.) and approximately 49%from the module assembly part (iii) (i.e. glass, EVA, metal frame, j-box, equipment, labor, cost of capital, manufacturing margin, etc.). In the cell cost (ii), the raw material accounts for more than 40 percent and nowadays, the silver paste consumption per standard silicon solar cell (i.e. $156x156mm^2$) influences for about 30% of the total cell cost (ii). Accounting for about 12% of the overall silicon solar cell cost (i+ii+iii). The main effort for solar cell metallization is to remove the silver paste and use cheaper metals (i.e. copper) [1].

The International Technology Roadmap for Photovoltaics (ITRPV), in March 2013 [1] estimates a reduction of silver paste for the 156x156 mm^2 cells from 150mg/cell in 2013 down to 50mg/cell in 2020. The beginning of such replacement on a large-scale basis must start in 2015. Before the introduction of copper alternative metallization techniques, technical issues in reliability and adhesion have to be solved and also appropriate production equipment has to be available as well.The solution that many companies are still chasing and trying to fix is light-induced plating (LIP) techniques. LIP have been well characterized and used for many decades [2,3,4]. LIP is referred to be a self-aligned metallization scheme due to the fact that “in principle” metal plates only in areas where the silicon is exposed [5]. In practice one of the main issue of LIP technique is the plating in pin-holes and scratches that are always present in industrial solar cell production line and the only solution to overcome such problem is to use inkjet patterning [6,7,8] by a resist material that will protect the cell during the LIP process.

Throughput in PV production line must be higher than 1000 cells/hour and the use of any kind of photoresist and/or resist process is not considered a feasible PV industrial solution. The ideal solution will be to perform selective localized plating touching the cell only where the process is needed by a mask-less technique. Furthermore, the foot print of the equipment must be kept as much compact as possible and to warrant high throughput the plating speed must be increased respect LIP process in which the maximum current density is in the range of 6 to 30 mA/cm^{-2}.The highest deposition rate for electroplated copper, to author knowledge, is 5µm/min [9]. In electroplating, the material deposition rate is governed by the Faraday’s law:

$$d_r = \frac{iM}{nF\rho S} \tag{1}$$

where d_r is the deposition rate, i the electro-deposition current, M and ρ the molar mass and the mass density of the deposited material respectively, n is the number of electrons per ion, F the Faraday constant and S the surface area of the deposit. Evidently, the amount of deposition is proportional to the current (eq. 1). High-speed plating requires high current, but cannot be increased indefinitely. Therefore, it is desirable to apply the maximum allowable current as one of the controlling electroplating parameters. The limiting current is given by:

$$i_{\max} = \frac{nFDS}{\delta} c_b \tag{2}$$

where i_{max} is the maximum current, D the diffusion coefficient of the deposited species, c_b the bulk concentration of the ions in the solution and δ the diffusion layer thickness. At value of the maximum (limiting) current the metal ions are reduced as soon as they reach the electrode. The limitations on current are influenced by mass transport phenomena at the cathode. Exceeding such maximum current leads to burnt deposits due to the depletion of cations in the vicinity of the cathode. The diffusion from the bulk solution is not fast enough. Hydrogen ions are reduced instead. This can be overcome by reducing the thickness of the diffusion layer (δ) [10].

The limiting current can be increased by:

- Hydrodynamics: velocity of the electrolyte flow (e.g. jet plating, rotating electrode, ultrasonic agitation);
- Temperature: Brownian motion, laser plating,

- Current distribution: Pulse plating, anode–cathode configuration;
- Bath chemistry: metal concentration, additives.

These expedients result in the reduction of the diffusion layer thickness.

Using laser-jet electroplating technique, record of copper deposition rate up to 50μm/s (i.e. 3000μm/min) with current density of $150Acm^{-2}$ were demonstrated [11]. Furthermore, it was found that the plating rate was relatively unaffected by the laser power that mainly improved the morphology of the deposit. Due to the high impingement flow of the liquid (i.e. meter per second) the main issues for such equipment will be resist erosion and how to limit and to contain the splashes of the liquid. Sub-0.10μm Cu interconnects already uses in principle a jet plating technique but both wafer and anode/jet assembly are immersed in the electrolyte to remove splashes [12]. Nowadays, jet plating in air is mainly used in reel-to-reel plating equipment for the PCB industry with a maximum deposition rate of 16μm/min [13].

The ideal solution, for the PV industry, will be to perform a mask-less selective localized jet plating aligning the wafer only where the copper must be grown.

Localized electrochemical deposition (LECD) has been introduced in Ref. [14] in which a conducting micro-electrode is used to fabricate high aspect ratio metal structures. Localized deposition is produced by placing an electrode tip, which has micrometer dimensions, near a substrate in an electrolyte and applying a potential difference between them. Due to the highly localized electric field in the region between the micro-electrode and the substrate, confined deposition is produced. In any case, there is a severe spreading at the columns bases, which limits the resolution of the LECD technique [15]. A liquid static meniscus obtained by a micropipette in close proximity to the substrate solves the spreading problem of the LECD technique. Wire dimensions down to 100nm where obtained [16]. A static liquid drop is formed at the end of the micropipette, and as the liquid drop gets in contact with the substrate surface, a static liquid meniscus is formed spreading on the surface depending on the wetting angle. As the dimensions get bigger gravity will influence and, the micropipette, with all the liquid inside, must be fully closed or as the liquid touches the substrate surface, the liquid will spread out until a new equilibrium will be reached between surface tension and gravity. Static meniscus impose tight control on the distance between micropipette and substrate due to finite quantity of liquid in the meniscus. Increasing such distance will break the formed meniscus. Furthermore, with a static meniscus is impossible to have mixing of the solution and this will limit seriously the deposition speed and decrease the morphology characteristics of the deposit.

2. The dynamic liquid drop/meniscus

To overcome the problem of static liquid drop/meniscus and to allow a continuous refreshment of the chemical solution is proposed as a new approach [17] based on a confined dynamic liquid drop/meniscus.

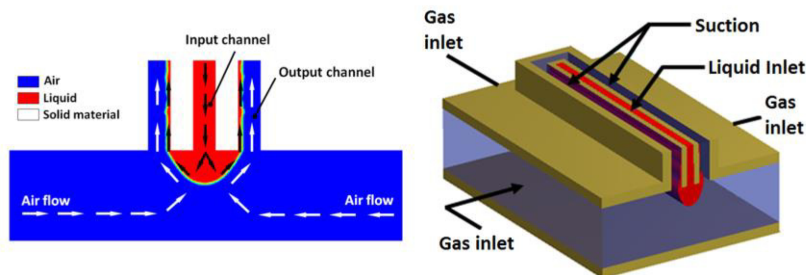

Fig. 1. (left) 2D scheme of dynamic liquid drop formation; (right) 3D scheme of rectangular shape DLD formation

Figure 1 (left) presents the 2D view of how the dynamic liquid drop (DLD). The system is composed, in a principle implementation, by an internal jetting outlet where a liquid flow is forced, and an external recalling inlet

where a depression (e.g. obtained by a vacuum pump) where the liquid is recalled back into the system. The input channel, that could be of any shape (e.g. circular, rectangular, etc.), confined by rigid wall (i.e. solid material), pumps a constant liquid flux that, depending on the input nozzle dimension, fixes the velocity of the liquid exiting the input channel. Due to a lower pressure in the surrounding of output channel, the airflow (gas) sustains the liquid (figure 1 left: black arrows in the red liquid) forming a DLD. The dynamic characteristics is due to the constantly refreshment of the liquid, during time, inside the drop. In figure 1 (right), is presented a schematic view of a 3D DLD for a rectangular input structure.

As the substrate gets in contact with the DLD, a dynamic liquid meniscus (DLM) is formed, as shown in figure 2. The contact angle will depend on the wettability of the surface. Once the DLM is formed, keeping constant all other parameters (i.e. fluid velocity and pressure), moving the nozzle closer or farther the DLM will always keep its shape.

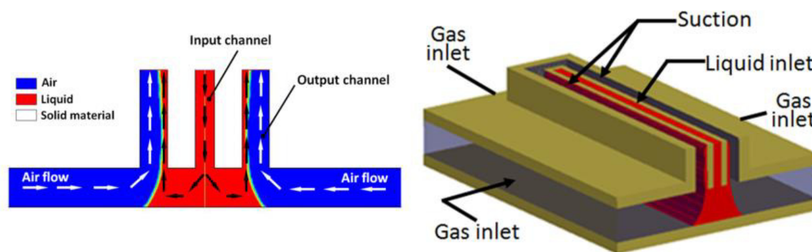

Fig. 2. (left) 2D scheme of DLM formation; (right) 3D scheme of rectangular shape DLM formation

In figure 2 (right) the situation when a rectangular DLD touches a substrate is shown. In the same figure are shown the output cannels (i.e. suction) and from where arrives the airflow (i.e. gas inlet).

The main different of DLM respect static meniscus can be well understood looking to the Computational Fluid Dynamics (CFD) reported in figure 3 where is shown the evolution in time (from a to f) of the DLM formation from the DLD as the substrates reaches the drop.

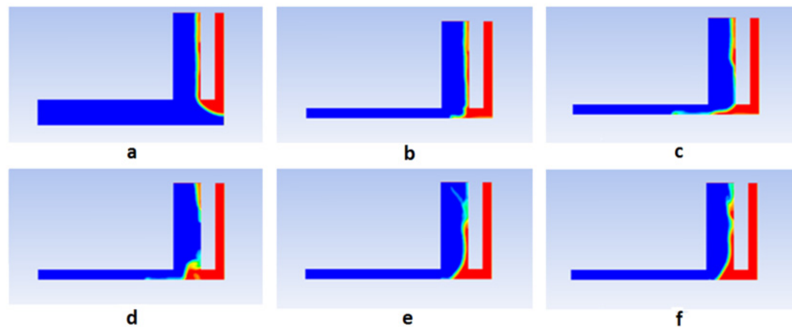

Figure 3. in red the DLM formation from DLD is shown: a) stable DLD formation, b) substrate in contact with DLD squeezing the drop, c) spreading of the liquid on the substrate surface, d) spreading liquid being recalled from the airflow in the output channel, e) the liquid spread on the bottom surface is totally recalled inside the output channel and the DLM is formed, f) the DLM is reaching is stable configuration with the liquid flowing on the output channel wall.

As can be seen looking at figure 3, during time, due to the airflow entering the output channel, any liquid spreading on the substrates surface will be pushed back and inhaled inside the output channel confining the liquid as shown in figure 2. In a static situation the liquid spreading on the surface will be lost. The transitory time,

shown in figure 3.a to figure 3.f, will depend on the dimension of the structures in any case for nozzle dimension in the order of millimeter the transient will last few milliseconds and in the range of few microseconds when the nozzle dimension are around tens of microns.

2.1. CFD Simulation

In low dimension (e.g. sub-millimeter) multiphase fluid flow, even if in operating configurations relatively simple, the phenomena becomes considerable complex and is necessary to solve the problem by using numerical CFD techniques available also by commercial software.

In the present work all the analyses have been done using the commercial software FLUENT 12.1.2 with the accomplishment of 2D axial symmetry and/or 2D planar and full 3D CFD models. Since we are interested in the mechanism of the DLD and DLM formation (i.e. multiphase flow) and that, in most of the studied cases the dimensions involved are sub-millimetric, the CFD models where developed in analogy of a ink jet printer nozzle.

Since, in the correct operation of the nozzle, is expected a net separation between the liquid phase and the gas phase, following what reported in [18, 19], the so called volume-of-fluid method (VOF) has been recognized as the suitable model to treat the problem of two or more immiscible fluids looking "to capture" the surface interface between the different phases. In the operating conditions, in which the nozzle must work (i.e. small dimension and relatively low speed of the fluids), it is expected a flow regime characterized by low Reynolds (Re) numbers (i.e. Re number for liquid not higher than 450 and Re number for gas not higher than 1500). This allows to assume a laminar viscous flow model for both of the phases involved in the simulation. Furthermore, considering that surface tension plays a key role at the interface between gas and liquid [20], in all the CFD models used the surface tension was taken into account using the value of 0.073N/m. It was also taken into consideration that the contact angle that the liquid phase forms with the solid walls that confines the studied multiphase flux: in the case of DLM the contact angle with the bottom wall was fixed to 53 degree.

The fluid dynamic problem has been solved adopting a spatial discretization scheme of the second order (i.e. to minimize the numerical error propagation). The step of temporal discretization has been chosen as a function of the dimensions of the nozzle to analyze, also considering that the employed VOF model is limited.

The standard algorithm Iterative Time-Advancement Scheme [21] has been chosen for the temporal evolution, and for each internal temporal discretization, the iteration number has been fixed to 20 or 30, depending on the model under simulation: 2D or 3D. Such number of iterations revealed to be more than sufficient to warranty residues converge up to 6 orders of magnitude for the continuity and momentum equations.

All simulation were performed on supercomputer LAGRANGE - HP Cluster Intel Xeon [22] using 128 cores (Intel Xeon QuadCore @3.166GHz) employing more than 15.000 hours of computational time.

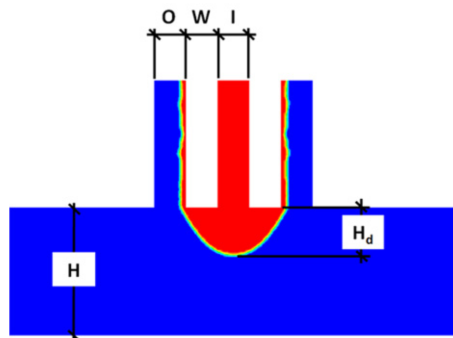

Figure 4. 2D scheme with defined I=inlet channel, W=wall dimension, O=output suction channel, H=distance of substrate, Hd=height of DLD.

In figure 4 and table 1 the 2D geometry and the simulated results with dimension of the nozzle going from 500 microns down to 15 microns are respectively presented.

Table 1. Geometry value and simulation results

I (µm)	W (µm)	O (µm)	H (µm)	V_{inlet} (ms^{-1})	Δp (Pa)	Re_{Liquid}	H_d (µm)
500	500	500	2000	0,45	1000	437	733
300	300	300	1000	0,5	1500	291	573
100	100	100	600	0,8	2000	155	213
70	70	70	600	0,9	2500	122	187
50	50	50	300	1	3000	97	118
30	30	30	200	1,25	3500	73	73
15	20	20	75	1,5	4000	44	32

The 5th column shows the velocity of the liquid and as can be seen they are all in the 1 ms^{-1} range. A jet-plating condition has been already reached when the speed of liquid is higher than 0.2ms^{-1}. The depression imposed (i.e. 6th column) to the suction channel has been fixed in order to warranty also a low Re number (i.e. lower than 2000 for the gas) and also to reduce the air mass flow system consumption. From the 7th column of Table 1 it can be seen that assumption of laminar flux is well confirmed (i.e. Re < 2000). The 8th column of Table 1 reports the height of the DLD. It must be considered that DLD height can be increased decreasing pressure difference at the suction channel and increasing velocity of liquid. The maximum velocity obtained, in order to form a DLD, for a 50 micron inlet channel (I), has been of 2.4ms^{-1} with depression of 50 000 Pa. Further increasing the velocity as also increasing the pressure, the airflow was not be able to sustain the liquid and no DLD was formed.

In the case of multiple DLD and DLM to warranty the necessary airflow to sustain the liquid, is necessary to insert an air-feeding channel. In figure 5 is shown a 2D DLD formation with 4 hanging DLD and the DLM for one of the DLD. The arrows in the figure 5 are indicating the flow of the air feed.

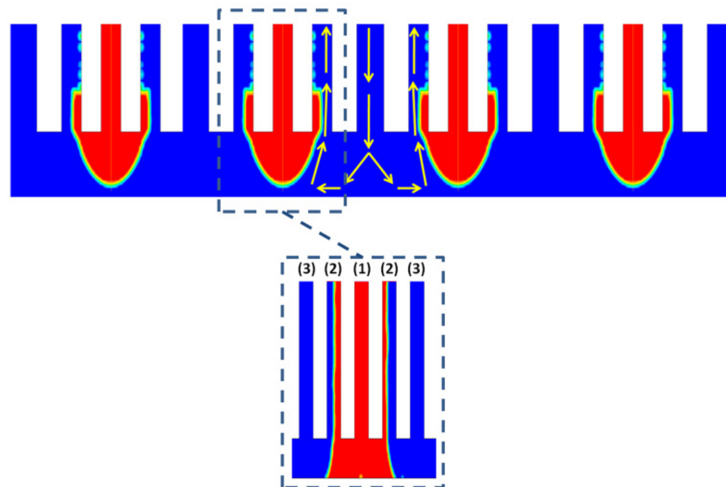

Figure 5. Multiple DLD and DLM. Liquid input channel (1), Suction output (2) Input airflow channel (3)

2.2. Experimental Testing and CFD validation

In table 2 the simulated values (CFD) and the measured values (TEST) ofthe realized prototype are reported. The results are in good agreement. In the last row the air consumption for the 4 rectangular nozzles of 3cm in length is reported.

Table 2. Comparison between CFD simulation and tested prototype.

	I (μm)	W (μm)	O (μm)	H (μm)	V_{inlet} (ms^{-1})	Δp (Pa)
Nozzles operating conditions	500	500	500	2000	0,4	2000
	TEST			**CFD**		
Dynamic drop height (μm)	570			590		
Dynamic meniscus footprint (μm)	1710			1760		
Air volume flow rate (l/min)	60,5			63,9		

Bringing the DLD in contact with substrates, as predicted by CFD, a DLM is formed. A glass substrate with a printed millimeter ruler has beenused and put in contact with the DLD. In figure 6 is presented an image of the 4 DLM with a zoomed inset showing a part of the DLM. From the zoom inset is possible to determine the dimension of DLM.

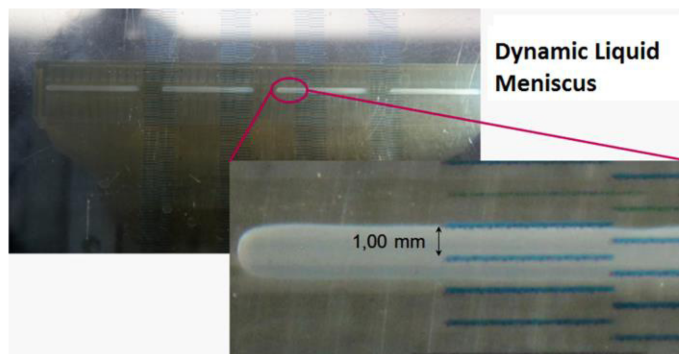

Figure 6. Image of the 4 DLM of 3 cm length. In the zoomed image details of DLM dimension.

The mechanics of DLD formation has been obtained by first applying the pressure at the output channel and then switching on the pumping system of the liquid input inlet. In this way no liquid has been lost and DLD has been formed. As the DLD is formed the substrate can be brought in contact by moving the nozzle head or the substrate or by a combination of them. As can be seen in figure 7 (left), if the substrates enter from (x) direction, as in a tape reel system, the DLM is formed as soon the substrate will touch the DLD. In this way it is possible to perform different way of processing:

1) Continuous process, in which the nozzle head is fixed and the substrates moves continuously under the nozzle head. Such technique has been tested on substrates kept by vacuum on a belt conveyer with speed up to

$20cms^{-1}$ without loss of drops. This technique is suitable for the PV industry especially for the metallization of fingers and bus-bars.

2) Stop and go process: in which the substrates or the head moves up in the (z) direction to form the DLM, stops and, as an example, the plating process can start. As finished, the DLD forms again moving away the substrate in (z) direction and then by moving in (x) and/or (y) direction with speeds up to tens of ms^{-1} substrate gets positioned in a new processing site. Such technique, following a step and repeat process, is also suitable for the PV industry.

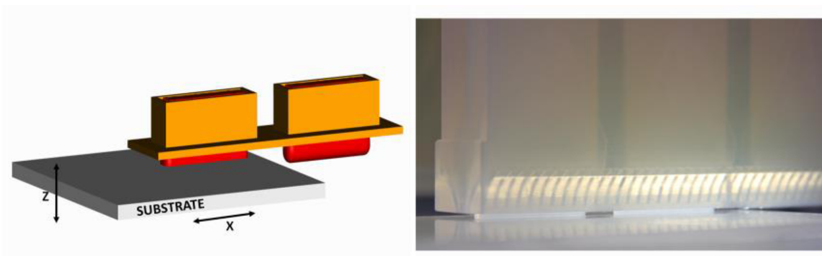

Figure 7. Image of the 4 DLM of 3 cm length. In the zoomed image details of DLM dimension.

Figure 7 (right), shows a real situation in which the substrate gets in contact with the first two DLD forming two DLM. In the same figure it can also be seen that the 3rd DLD is almost getting in touch with the substrate.

In figure 8 an optical image,5x zoomed, of the footprint shape left from the DLM after a stop and go cleaning process on a dirty silicon wafer is shown.

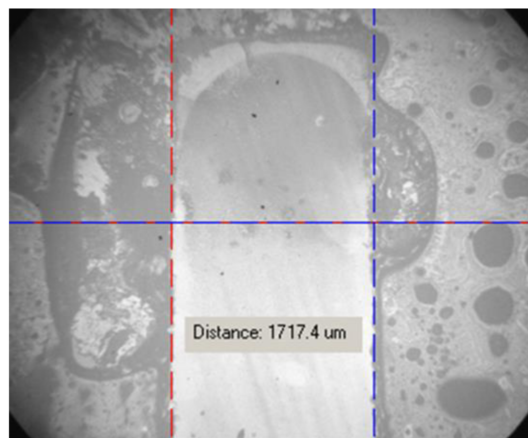

Figure 8. Footprint of the DLM left on the wafer.

By using such new technique, plating of copper has been performed on mono-crystalline silicon solar cell using a standard industrial acid solution with ion copper concentration of 75g/l and applying a current density of $0.5A/cm^2$achieving a deposition rate of 9µm/min [29]

3. The dynamic liquid drop/meniscus applied to silicon solar cells

The new technique allows to perform any type of wet processes without need of lithography. Such new technique allows the front and/or the back surface of a solar cell to be touched only in specific defined positions. Using this technique is possible to open silicon nitride fingers and bus bar chemically without lithography, perform electrochemical plating in a localized manner and intensify deposition rate of metals, since DLM have speed of

liquid flow like in a jet-plating technique. The adhesion problem of metal (i.e. Ni) directly plated on silicon solar cell is solved by introducing a porous silicon formed by DLM. The different configurations of DLM used for localized wet treatment of silicon solar cellsare presented in figure 9.

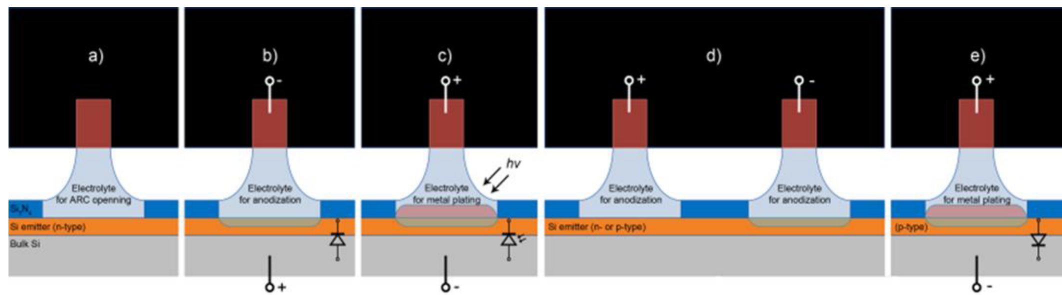

Figure 9. DLM steps: a) opening of ARC layer, b) PS formation in emitter region of n-type conductivity, c) electroplating onto the PS region made on emitter of n-type conductivity, d) PS formation suitable for emitters both of n- or p-type conductivity, e) electroplating onto the PS region made on emitter of p-type conductivity

Nanostructured PS is usually obtained by electrochemical etching (anodization) of silicon crystals in an electrolyte containing HF. The substrate doping, crystallographic orientation, electrolyte composition, and current density are the process variables that affect PS morphology and, thus, its electrical and mechanical properties. A layer of nanostructured silicon with gradient porosity, with a thickness less than 50 nm, with respectively 400 nm of nickel and 9 micron of copper electrodeposited layers showed adhesion strength of more than 5N/mm.

The electrical contact between nickel and silicon depends on silicon resistivity and the Ni work-function that is 0.52 eV. Since nanoporous silicon is used, the key point to obtain low specific contact resistivity is to fill totally the pores of porous silicon with Ni. We remark that a partial filling of the pores increases the specific contact resistivity due to the high resistance of the porous silicon structure. The main process to warranty good adhesion and a full pore filling is to form porous silicon with a gradient porosity and deposit Ni by PRP (Pulse Reverse Plating) technique. As can be seen from the SEM cross-section micrograph of the nickel films deposited onto nanostructured PS gradient layer, shown in figure 10, depending on Ni plating regimes, the pores can be only partially filled. In the cross-section micrograph of figure 10 we show: a) current density versus time is constant,; b) current density is linearlyincreased versus time; c) PRP (Pulse Reverse Plating) at low current densities (j_{dir} = 20 mA/cm^2j_{rev} = 4 mA/cm^2); d) PRP at high current densities (j_{dir} = 100 mA/cm^2, j_{rev} = 20 mA/cm^2).

The only way to warrant a complete filling of pores is to perform a gradient PS regime formation and a first step of PRP of Ni.

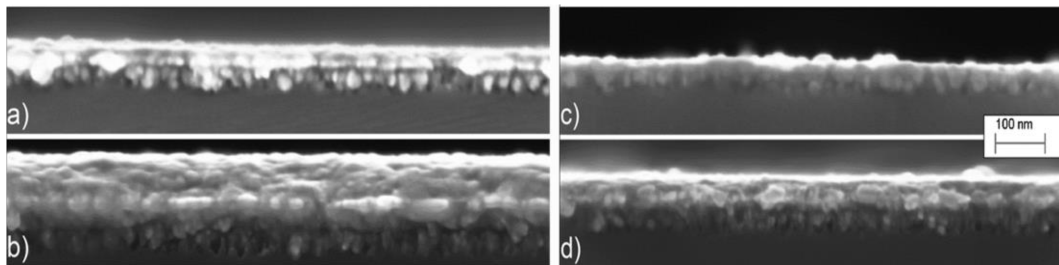

Figure 10. SEM cross-section micrograph of Ni filling porous silicon under different plating regimes: a) current density versus time is constant, b) current density is linearly increased versus time, c) PRP (Pulse Reverse Plating) at low current densities d) PRP at high current densities.

In figure 11 (left) a SEM cross-section after annealing at temperature lower than 400°C for 20 minutes is presented. No porous structures is present in the Ni silicide layer, 45.90 nm thick. In figure 11 (right) is shown the peel test adhesion of Ni – Si structure.

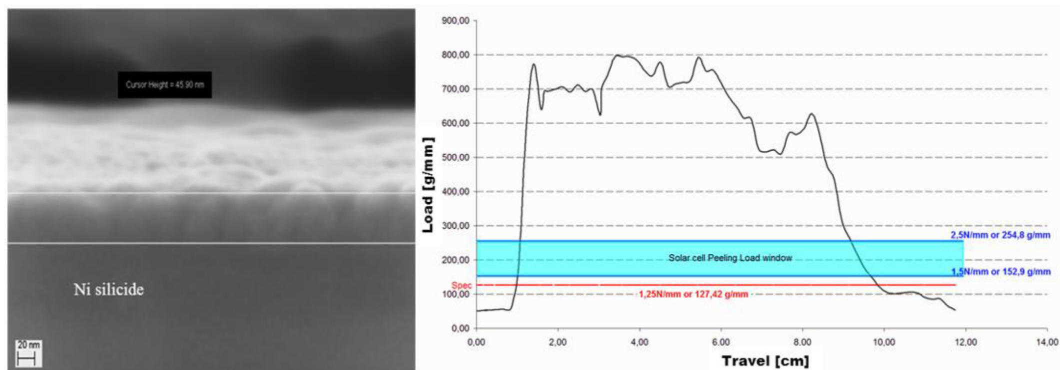

Figure 11. (left) SEM cross-section micrograph of Ni silicide formed after annealing of totally filled porous silicon with Ni by PRP. (right) Peel test adhesion of annealed plated Ni on silicon using porous silicon as anchoring layer.

In figure 12 is shown the final structure of the metallization stack obtained after Ni silicide formation at temperature below 400°C and copper plating processes. Annealing procedure and further plating of Cu do not affect the quality and homogeneity of Si/Ni interface, which is the critical point. Indeed this interface is responsible for both electrical and mechanical properties of the entire metallization stack.

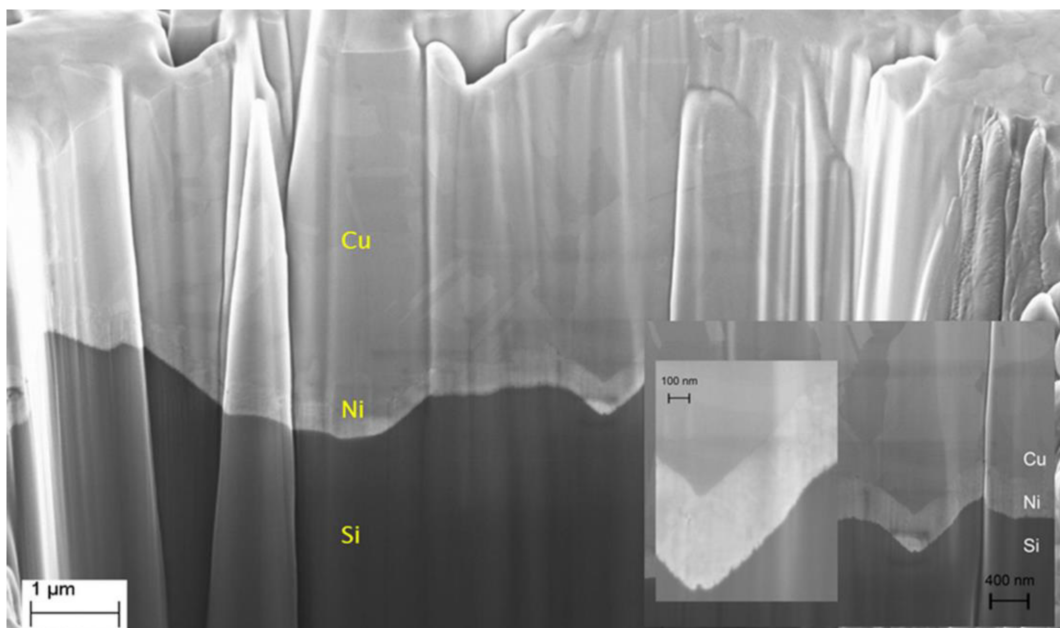

Figure 12. SEM cross-section by Focus Ion Beam showing the Si-Ni-Cu structure. The zoomed inset shows the porous silicon totally filled by nickel.

Table 3: Specific contact resistivity measured by TLM (Transfer Length Method) after Ni silicide formation at temperature lower than 400°C

	Specific contact resistivity [Ohm cm²]	Sheet Resistance [Ohm/sq]
Ni partially filling the pores of PS	> 4•10^-3	50-60
Ni partially filling the pores of PS	> 5•10^-3	70-80
PS with gradient and complete Ni filling of PS pores	340 ÷ 420 · 10^-6	50-60
PS with gradient and complete Ni filling of PS pores	500 ÷ 550· 10^-6	70-80

In table 3 the specific contact resistivity for different emitter resistivity are reported. As can be seen from table 3 an incomplete filling of the porous silicon leads to a higher specific contact resistivity.

Current-Voltage characteristics of the cell in dark and room temperature after stress-annealing [23] showed that Ni is a perfect barrier layer to copper. After the first two stress-annealing steps (300°C and 350°C respectively) an improvement was evident (current densities reduction in both reverse and low forward bias conditions). A further thermal annealing stress at 400°C for 1 hour destroyed the junction. Following Arrhenius model is possible to estimate that 100 hours at 200°C are equivalent to 4 hours at 275°C or 1 hour at 350°C. A. Mondon estimated that 100 hours at 200°C are equivalent to 100 year of normal working temperature of solar cell [24].

Table 4: Comparision of 4x4cm² solar cell with different back contacts

Sample	Voc [mV]	Jsc [mAcm⁻²]	Normalized FF	Normalized Eff	Rs [Ωcm²]
S29 - Al contact	625	36.3	1	1.000	2.3
S29 - Ag contact	586	34,6	0.782	0.700	3.0
S29 - Sn contact	624	36.1	0.992	0.992	2.3
S30 - Al contact	628	35.4	1	1.000	2.9
S30 - Ag contact	590	34.5	0.825	0.756	3.0
S30 - Sn contact	628	34.7	0.998	0.980	2.8

The Al back side of the solar cell were also treated with the selective process and after a special treatment on the fired Aluminium paste, Tin is directly deposited and peel test showed adhesion higher than silver on silicon (i.e. > 1N/mm). Different solar cell $4x4cm^2$ were realized in order to compare characteristics respect a full Aluminium back contact and an Aluminium and Silver back contact. As can be seen in table 4 Tin contact directly on Aluminium doesn't damages the solar cell and increases efficiency respect a back silver contact. S29 and S30 are the two different solar cell realized and they differ only for the back Al paste: S29 has small Al particles and S30 has big Al particles.

Conclusion

A new selective processing technique based on a confined dynamic liquid drop\meniscus is presented showing as this new technology could be applied to industrial solar cell production in order to replace silver paste with Nickel Copper from the front and the back side of silicon solar cell. The main mechanical and electrical characteristics for the front and back side removal of silver paste are evaluated and presented showing that the new technology can perform selective wet processes suitable for industrial manufacturing of a silicon solar cell.

References

[1] International Technology Roadmap for Photovoltaics (ITRPV) Edition March 2013.

[2] I.A. Lesk, R. Pryor, Method of Semiconductor Solar Energy Device Fabrication, Patent No. 4557037, United States, 1978.

[3] S.R. Wenham, M.A. Green, Self Aligning Method for Forming a Selective Emitter and Metallization in a Solar Cell, Patent No 6429037, United States, 2002.

[4] J.H. Guo, J.E. Cotter, Metallization improvement on fabrication of interdigitated backside and double sided buried contact solar cells, Solar Energy Materials and Solar Cells 88 (2005) pp. 485–498.

[5] S. Wenham, Buried contact silicon solar cells, Progress in Photovoltaics (1993) pp. 3–10.

[6] A. Lennon, R. Utama, A. Ho-Baillie, S. Wenham, Inkjet method for direct patterned etching of silicon dioxide, Proceedings of the Digital Fabrication Conference, Pittsburgh, USA, 2008, pp. 251–254.

[7] R. Utama, Inkjet printing for commercial high-efficiency solar cells, Ph.D. Thesis, Center of Excellence for Advanced Silicon Photovoltaics and Photonics, University of New South Wales, Sydney, Australia, 2009

[8] D. Hua, R. Barr, P. Hinkley, Inkjet plating resist for improved cell efficiency, Photovoltaic Specialists Conference (PVSC), 2010 35th IEEE; pp. 2142-2146

[9] B. Wei Koh, Lin, Process development for high-current electrochemical deposition of copper pillar bumps, 62nd IEEE Electronic Components and Technology Conference (ECTC), 2012, pp. 630-635

[10] M. De Vogelaere, V. Sommer, H. Springborn, U. Michelsen-Mohammadein, High-speed plating for electronic applications, ElectrochimicaActa 47 (2001) pp. 109–116

[11] R. J. von Gutfeld and D. R. Vigliotti, High-speed electroplating of copper using the laser-jet technique, Appl. Phys. Lett. 46, (1985), pp. 1003-1005

[12] M. De Vogelaere, V. Sommer, H. Springborn, U. Michelsen-Mohammadein, High-speed plating for electronic applications, ElectrochimicaActa 47 (2001) pp. 109–116

[13] U. Cohen, G. Tzanavaras, Jet ECD plating and seed layers for sub-0.10µm Cu interconnects, Solid State Technology, Magazine Articles, 1 May 2001

[14] Hunter I W, Lafontaine S R and Madden J D 1997 US Patent Specification 5,641,391

[15] R. A. Said, Microfabrication by localized electrochemical deposition: experimental investigation and theoretical modelling, Nanotechnology 14 (2003) pp. 523–531

[16] Jie Hu and Min-Feng Yu, Meniscus-confined three-dimensional electrodepostion for direct writing of wire bonds, Science, 329 (2010), pp. 313-316

[17] M. Balucani, Photovoltaic cell with porous semiconductor regions for anchoring contact terminals, electrolytic and etching modules, and related production line, WIPO Patent Application WO/2011/110682

[18] T. Glatzel, C. Litterst, C. Cupelli, T. Lindemann, C. Moosmann, R. Niekrawietz, W. Streule, R. Zengerle, P. Koltay, Computational fluid dynamics (CFD) software tools for microfluidic applications – A case study, Computers & Fluids 37 (2008) pp. 218–235

[19] C.W. Hirt, B.D. Nichols, Volume of fluid (Vof) method for the dynamics of free boundaries, J ComputPhys 39, (1981), pp.201–225

[20] T. Lindemann, Droplet Generation From the Nanoliter to the Femtoliter Range, Ph.D Thesis, Freiburg i. Br., July 2006

[21] ANSYS FLUENT 12.0 Theory Guide, April 2009

[22] http://www.cilea.it/index.php?id=lagrange

[23] J. Bartsch, A. Mondon, K. Bayer, C. Schetter, M. Hoerteis, and S. W. Glunz, Quick determination of copper-metallization long-term impact on silicon solar cells, Journal of the Electrochemical Society. 157, pp. H942-946 (2010).

[24] A. Mondon, J. Bartsch, B.-J. Godejohann, M. Hörteis, S.W. Glunz "Advanced front side metallization for crystalline silicon solar cells based on a nickel-silicon contact" 2nd workshop on Metallisation for crystalline silicon solar cells, Konstanz, 15th April 2010, pp 42-47.